TECHNICAL MEMORANDUM

193

Synoptic cloudiness validation in the ECMWF model

N.G. Kvamsto

Research Department

August 1993

European Centre for Medium-Range Weather Forecasts
Europäisches Zentrum für mittelfristige Wettervorhersage
Centre européen pour les prévisions météorologiques à moyen

1. INTRODUCTION

In *Morcrette et al* (1991) radiation and cloud interaction processes are addressed. It was recognized that the present cloud scheme showed limited skill in providing the radiation scheme with realistic cloud distributions and optical properties of the cloud fields.

On this background a new, fully prognostic parametrisation scheme for cloud- and cloud associated processes in the ECMWF model has been developed by *Tiedtke* (1993).

In this report a synoptic validation of the performance of the present operational and the new scheme will be presented. The objective of the comparison is to reveal differences between the schemes and through these show to which extent the new scheme represents an improvement. The investigation is also an attempt to provide information of how any deficiencies of the schemes may be linked to the large scale flow.

The (verification) datasets available for a synoptic day to day validation of cloudiness are infrared and visible satellite imageries and conventional synop observations. Apparently, a more precise and quantitative validation may be carried out by calculating model radiances in the satellite channels and comparing them with the measured radiances. However, any differences between the two radiance fields may be due to: a) Unrealistic cloud cover, b) unrealistic optical properties, c) unrealistic vertical distribution of clouds, d) deficiencies in the parametrisation of radiative transfer in clouds. Hence it is advantageous to compare model cloudiness with clouds "retrieved" from satellite radiances as well as radiances directly. Such a validation may help to reduce the ambiguity of any quantitative comparison. The disadvantages of a synoptic validation are that global mean and time integral properties will not be addressed.

Nine cases over Europe in 1993 have been selected for the cloud validation; 15 - 18 January, 14 February and 22-25 June. After a short description of the cloud schemes the results will be presented in the following sections.

2. THE CLOUD SCHEMES

Both schemes allow clouds to be present in any model layer but the lowest.

The operational cloud scheme is entirely diagnostic, ie it is the cloud fraction itself that is parametrized. Cloudiness associated with convection (cumulus clouds and anvil cirrus) is a function of the scaled time-averaged precipitation rate. The stratiform cloud fraction is mainly a function of relative humidity. Inversion cloudiness is expressed in terms of the vertical temperature gradient and relative humidity. A detailed description of the scheme is given in *Slingo* (1987), although the scheme has subsequently been adjusted in several aspects.

The new scheme introduces the fractional cloud cover as a prognostic variable, the parametrization being now in source and sink terms of cloud mass rather than the cloud fraction itself:

$$\frac{\partial a}{\partial t} = A(a) + \sum_i S_i$$

where A denotes the advective terms and S_i denotes the sources and sinks. For further details see *Tiedtke* (1993). It should be mentioned that experiments with the new scheme investigated in this paper has been performed with no advection (ie the A terms are set to zero).

3. A SYNOPTIC ASSESSMENT OF THE OPERATIONAL CLOUDINESS FORECASTS OVER EUROPE DURING THE WINTER CASES

The examples in this section will be taken from the January period.

Datasets available for such a validation are infrared and visible satellite imageries from Meteosat and conventional synop observations. Those data are available at 00, 06 12 and 18UTC for each day in the selected period. The observation times are chosen to correspond to the 36, 42, 48 and 54h forecast, respectively. During this period significant baroclinic activity took place over the selected area.

3.1 Frontal clouds

The cloud belts in a mature cyclonic system are associated with the general (moist-) isentropic motion within the cyclone. In the frame of reference moving with the system, well defined airflows appear. The ascending airflows are often referred to as conveyor belts. Schematically, the warm conveyor belt (WCB) is formed as air originating at lower levels in the warm sector equatorward of the surface low, rises as it flows along the cold front and splits into two branches, one cyclonic and one anticyclonic. This region is often referred to as the "hammer head". Condensation occurs as the warm sector branch is rising, thereby triggering cloud formation and enhancing cross isentropic motion. Thus, the WCB is the primary cloud producing flow. Another well defined cloud and precipitation producing flow of this kind is the cold conveyor belt (CCB), often not as distinct and extensive as the WCB. Originating in the anticyclonic low level flow to the north east of the cyclone, the air in the CCB travels westward (relative to the eastward moving cyclone) just ahead of the warm front undercutting the WCB and moves along the back-bent warm front (occlusion). For a more complete and detailed description see *Browning* (1990), *Carlson* (1991) ch 12 and *Thorncroft et al* (1993).

a) Predicted horizontal distribution of frontal clouds

An impression of the model's skill in predicting the horizontal distribution of the high clouds may be obtained from Fig 1. One can see from the 95% contour of the high cloud cover (HCC) in the model that the WCB associated cloudiness is correctly placed in the horizontal. However, the cross frontal extent of

solid high clouds is overestimated almost everywhere, except in the hammer head region. In this region it seems to be an underestimation of the horizontal extent of the cloudiness. This impression may be supported by plots such as Figs 1 and 2 throughout the periods.

As mentioned the CCB is often less extensive than the WCB. Following the conceptual cloud models of mid-latitude weather systems (see *Browning*, 1990 and *Carlson*, 1991), clouds produced in the CCB may nearly always be associated with the occlusion, when seen in the horizontal plane. (The warm frontal part may often be hidden by the high clouds of the WCB). During the selected period, the model reproduces quite well the extent of the cloud belt on the occlusion, s. Fig 2.

A wave that enters the selected area about 15 January 12UTC is associated with a CCB starting just ahead of the WCB hammer head. However, as the leading surface ridge makes landfall (16 Jan 12UTC) the imageries indicate that there are low level layered clouds along the warm front in the anticyclonic region. Both the relevant bias maps (not shown) show that most of these low level clouds are absent in the model.

The only period in which significant convection occurs over land is 15 January 06UTC to 16 January 00UTC over central Europe in connection with a warm front passage. The observers have reported altocumulus (mid-level convection). The altocumulus clouds can be seen in Fig 1 (and 4) over England (6 hours before the system reaches the continent). The corresponding CCC fields (eg Fig 2c) indicate that the midlevel convection is absent in the model. Twelve hours later this deficiency can also be seen in the bias field over central Europe (Fig 3).

b) Predicted vertical distribution of frontal clouds

As mentioned, stratiform clouds are computed on the individual model levels. However, in the operational model the cloudiness fields are stored as Total Cloud Cover (TCC), High Cloud Cover (HCC) (450-100 hPa), Medium Cloud Cover (MCC) (800-450 hPa), Low Cloud Cover (LCC) (1000-800 hPa) and Convective Cloud Cover (CCC) during the postprocessing. During the selected period, the model fields (eg Fig 2) show a rather general increase with height of the horizontal cross frontal extent of the cloud belts associated with the WCB. The model outputs also indicate that the fractional cloud amount increases with height, which implies that the lower clouds tend to be more broken than the fields aloft. Strictly one can not verify this model feature by the available "observations". Nevertheless, the infrared imagery indicates that the high cloud cover is quite broken equatorward of the "hammer head". Such an observation may be supported by the conceptual models, in which it is stated that cold dry air aloft is often crossing the WCB. The result is a potentially unstable lapse rate which may lead to convective clouds and a mixing of WCB air with that at higher levels. (When referring to the satellite imagery it is assumed that high clouds appear brighter than low clouds.)

3.2 Clouds in the northerly flow behind the cold front

a) Over sea

Often midlatitude weather systems are associated with a rather extensive area of convective clouds over sea in the northerly flow behind the cold front. The dynamic structure of this flow is described by *Økland* (1983). There are several examples of this phenomenon occurring during the selected period (see Fig 1). The aerial extent of convective cloudiness regime is captured quite well by the model (see Fig 2b), but both the imagery and ship observations indicate that the model rather systematically underestimates the fractional cloud amount (see Fig 3). These clouds are reflected both in the MCC and LCC fields, which implies that cumulus convection penetrates above 800 hPa.

b) Over land

As the cyclone makes landfall the characteristic cold air cumulus clouds disappear and are shortly replaced by low level layer clouds (see Fig 1). Convective clouds may occur, but not in an organized manner, as over sea. The model produces some low clouds in relevant areas (see Fig 2c), but the bias plots (Fig 3) indicate that the forecasted cloud amount is too small.

3.3 Clouds in the anticyclone

During the first one or two days of the selected period, the satellite pictures (see Fig 1) show a broken cloud belt stretching from the north west coast of Africa, along the Iberian west coast and eastward. Presumably this is the remnants of an old front that belonged to the low pressure system centred over Russia. By 16 January 00UTC most of this cloud belt has evaporated. This cloud belt is represented by the model mostly as high clouds. (The images indicate that there may exist lower clouds as well, in reality.) The break up process is quite poorly reproduced by the model, which leads to an overestimation of the cloud cover in this region at 15 to 16 January (see Figs 2a). The maximum error is located west of the Gibraltar strait. More or less the same situation occurs on 18 January. The model is not able to sufficiently break up the clouds at a front that has become inactive/passive. The error seems to be most pronounced in the upper layers.

The satellite pictures show that large areas in the western parts of the Mediterranean sea are covered with low layer clouds (maybe fog) during most of the period. The model outputs and synop observation shows that those clouds are systematically underestimated in the model, both with respect to horizontal extent and fractional cloud cover amount.

In the February case a high is centred over Russia. This anticyclone is surrounded of a rather broad belt of low clouds on the southern side. In the centre of the cyclone there are no clouds. The operational cloud scheme underestimates the amounts of low clouds in the southern cloud belt. On the other hand, the model

has produced significant cloud amounts in the centre of the anticyclone. These spurious clouds seem to be associated with an unrealistically strong temperature inversion.

4. RESULTS FROM RUNS WITH THE NEW SCHEME

Another set of forecasts (for the same period) has been carried out with the ECMWF model, in which the operational cloud scheme has been replaced by the new cloud scheme.

4.1 Horizontal distribution of frontal clouds

The overall impression is that the frontal clouds are quite well reproduced with the new scheme. Several detailed patterns are reflected in the model. However, there are also deficiencies. The most apparent and systematic one is an underestimation of the high cloudiness in the occlusion and "hammer head" regions (see Fig 4). It would be interesting to see if this deficiency would be reduced if advection of clouds mass included in the experiments with the new scheme. Furthermore, the cross frontal extent of HCC associated with the cold front in the Atlantic is too large (see Fig 4). In active systems this feature seems also to be the case throughout the rest of the period, but not to the same extent as in the opereational scheme. One should, however, note that the cloud cover is more broken than in the operational scheme, which is more realistic. The system over Russia, (see Figs 1 and 4) which has reached the decaying phase, has a too large area of solid HCC along the cold front in the operational model. The new scheme has produced a much lesser amount of HCC here, in fact the new scheme has produced most of this system's clouds in the MCC and LCC fields. The above-mentioned circumstances might suggest that there is a threshold problem in the operational scheme.

Like the operational scheme, the new scheme also seems to underestimate the low layer cloud extent along the warm front (see Figs 5 and 6), but to a far lesser degree than the operational scheme.

The previously mentioned midlevel convection (see section 3.1.1) that took place over central Europe 15-16 January is not forecasted by the new scheme either (See Figs 4, 5 and 6).

From 16 Jan 18UTC and onwards the new scheme overestimates the HCC and LCC in the poleward part of the warm sector.

4.2 Vertical distribution of frontal cloudiness

The model output (Fig 5) shows that there is no systematic trend in the variation of cloud extent and fraction with pressure. On the contrary, the conveyor belt clouds seem to have small variations between cloud top and cloud base. For the equatorward part of the WCB this seems to be well in agreement with

conceptual models, but in the "hammer head" region one should expect a decrease of cloud extent with pressure. Note that areas with a < 95% constitute the major part of HCC.

4.3 Clouds in the northerly flow behind the cold front

The new scheme seems to represent the observed cloudiness in this region quite well, both over land and sea. As was the case for the operational scheme, the convective cloudiness is reflected both in MCC and LCC (see Fig 5).

4.4 Cloudiness in the anticyclone

The previously commented (Section 3.3) inactive front in the first part of the selected period is associated with clouds that evaporate in an 18h period during 15-16 Jan. The evaporation process seem to take place in the model but the decay is too slow, this leads to an overestimation of the cloudiness over the Iberian west coast. Comparing the forecasts with the new and the operational scheme it is apparent that the cloudfields are more broken in the "new scheme" forecasts than in the operational ones.

Similar to the operational scheme, the low layer clouds/fog in the Mediterranean sea are systematically under-represented here as well, but not to the same extent. The new scheme also produces spurious clouds in the anticyclone over land in the February case.

4.5 Statistics

A more quantitative intercomparison between the model output and the synop observations is listed in this section. Fig 7 a) to c) shows that with respect to area averaged bias, standard deviation and correlation coefficient, the new scheme compares favourably with the operational scheme. The diurnal variation in Fig 7a) is thought to be due to the fact that it is difficult for the observer to estimate cloudcover at night and emphasises that the local noon observations are more reliable.

The absolute cloud frequency diagrams in Fig 8a and b shows that the operational scheme has a tendency to produce a fractional cloud cover value between 0 and 2 octas too often, and underestimates the occurrence of overcast conditions. A similar error pattern may be found for the new cloud scheme. However, the absolute error values are smaller here. Such diagrams give only information of frequency distribution within each data set. To obtain the number of points in each octa class that corresponds to the same class in the observed data set, one can calculate the surface and/or contour the cross frequency matrix. Such surface/contour plots are contained in Fig 9. From both Fig 9a and b one can clearly see that both schemes have forecasted points in the "wrong corners" of the diagram. In order to identify the flow type that might be associated with the points most distant from the (0,0) -(8,8) diagonal, one may split the data into different flow classes. One example/suggestion is given in Fig 9c and d where forecasts with the "new

scheme" of cloud frequency vs observed cloud frequency is split into one anticyclonic class and one cyclonic class. (The relative vorticity at 850 hPa is taken as the criterion). It is evident from Fig 9c that the majority of the cyclonic points have an observed cloud cover above 5 octas, whereas the forecasted cloud fraction covers the full range. Even though phase errors in the forecast and observation errors may cause spread in such diagrams, it is worth exploring the potential of this method.

The cloudiness bias frequency distribution may also be suggestive with respect to diagnosing forecast errors. The bias distributions for both schemes averaged over four 48h forecasts (15-19 Jan) are plotted in Fig 10. Except for the right hand tail, the new scheme is associated with a smaller amount of biases than the operational scheme. However, both cloudiness forecasts have the same distribution shape with three maxima. Some of the characteristics of the points in the tails of the bias distribution may be seen in Fig 11. The points which have bias > 5 octas (overestimated cloud amount), seems to be mostly low clouds (60%) in the new scheme case, whereas the operational scheme overestimates both high and low clouds. This difference between the two schemes is also reflected in the more subjective assessment of the two cloudiness forecasts.

In the opposite tail of the bias distribution low cloud base is observed at most of the points where the both schemes have underestimated the cloud amount by more than 5 octas (see Fig 12). One should be aware that the lowest significant clouds not necessarily constitute the dominant cloudy area. However, Fig 13 shows where those points are situated in the flow. This example shows clearly that the new scheme has improved the representation of low clouds behind the cold front over land. In order to have confidence in such an indication, the amount of investigated data need to be larger than in this example, both with respect to sampling time and area domain.

5. THE SUMMER CASES: 22 -25 JUNE 1993

Unlike the January cases, the flow has a more stationary character during the selected summer period. The flow pattern is characterised by a decaying low over Scandinavia and the north of Russia. There is a ridge (or high) in the north west Atlantic which is followed by a mid-latitude weather system south of Greenland. A frontal zone, which starts as a warm front of the western wave, surrounds the ridge on the western and southern edges. Furthermore, it goes across Europe, mostly along the 50°N latitude (with a weak S-N component), and splits over Russsia where the weak northward branch bends cyclonically into the decaying low (see Fig 14). During the next days this pattern will move slowly eastward and also a wave will develop on the front over south/central Europe.

In the assessment of the model cloudiness, we will refer to three main regimes: a) the anti-cyclonic flow associated with the north east atlantic ridge, b) the cold air behind the north eastern low and c) the frontal zone across Europe.

6. THE OPERATIONAL FORECAST

6.1 Clouds in the anti-cyclonic region

Judging from the satellite images (eg Fig 15), most of the cloudiness in this region seems to be low stratocumulus clouds. As one approaches the cyclonic flow off the Norwegian coast, the cloudiness becomes more convective. The extent of low stratocumulus cloudiness in the high is clearly underestimated during most of the selected period. Throughout the period the largest deficiencies are found in the north and in the northerly part of the flow around Iceland and southward to the British isles (see Fig 14a). In the southerly flow the model's low cloudiness has a realistic extent. The ridge seems also to be associated with spurious (excessive) high clouds (HCC) in the model.

6.2 Clouds in the cold air behind the north eastern low

Unlike the winter cases this flow regime is mostly associated with convective clouds (see Fig 15), both over land and sea. To some extent this is captured in the model which has produced CCC in the relevant places. However, the surface observations indicate that the predicted cloud amount is generally too small, especially at the 12Z observation. There is a distinct diurnal variation of the model cloud cover over land, with peak at 12Z. This coincides with the time of minimum negative bias in this region, which may indicate that the peak in CCC is too small. The convective cloudiness off the Norwegian coast does not have a diurnal variation, but the predicted extent of the convective area is too small. The CCC is also incorporated into the MCC and LCC during the postprocessing. Those cloud fields also have a diurnal variation over land with the same phase as CCC and the cloud cover values oscillate between 0 and [0.1 -0.25], which is more or less the same amplitude as in the CCC variation. That means that other cloud types that constitute LCC and MCC together with CCC do not have any diurnal variation. High cloud cover in this flow regime occur in connection with an upper level trough and the old occlusion associated with the decaying low (LCC and MCC as well). It seems that the model's upper level clouds are too solid and extensive.

6.3 Clouds in the frontal zone across Europe

There is a weak surface pressure depression on the frontal zone across Europe. Initially it is situated over the Alps and seems to be stable (see Fig 14), but as a disturbance aloft approaches at 24 June 0-6Z from the north, an unstable wave develops during the next day. Cloudiness associated with this disturbance, both during the initial and growing stages is quite generally underestimated. Low and medium cloudiness associated with the fronts in the developing system have the largest errors. Also the convective cloudiness behind the "new" cold front is clearly underestimated.

7. FORECASTS WITH THE NEW SCHEME

7.1 Clouds in the anti-cyclonic region over the North Atlantic

The cloudiness produced by the new scheme appears quite realistic. Several patterns in the satellite imageries can also be found in the model output. The excessive HCC in the operational forecast is not found here and the LCC in the northerly winds is also well represented. However, the broken character of the low clouds in the most southern parts of the ridge is not so well reproduced. The rather solid character of the LCC in the model leads often to an overestimation of the low clouds in those regions (see Fig 14b). Another deficiency is the underestimation of the low clouds around Iceland and between Iceland and the polar Ice edge.

7.2 Clouds in the cold air behind the north eastern low

The cloudiness associated with this flow regime is also well reproduced. The convective cloudiness off the Norwegian coast has a realistic extent and is represented mostly as LCC in the model. High- and midlevel clouds in connection with small disturbances, the old occlusion and the upper level low over southern Norway have large similarities with the satellite imageries. The rather homogeneous convective cloud cover over north eastern Europe seem to be well reflected in the MCC (and sometimes LCC) fields, even if there are small patches/clusters that are sometimes misplaced (see Fig 14b). Unlike the operational cloud scheme, the new cloud scheme does not produce any diurnal variation in the cloud fields. Since the MCC and LCC fields are a mixture of different cloud types, one can not exclude the possibility that different cloud types have diurnal variations with phase shifts which result in a constant MCC/LCC throughout the day. However, it is not possible to verify any diurnal variation from the available METEOSAT imageries (both IR and visible at day time and IR only at night time).

7.3 Clouds in the frontal zone across Europe

The high cloudiness associated with the disturbance on the frontal zone seems to be underestimated by the new scheme. The satellite images indicate also that some convective clusters in connection with the new fronts are absent in the new scheme. Otherwise the clouds in this system are represented well.

7.4 Statistics

Fig 16 shows some standard statistical quantities averaged over the chosen area. With only a few exceptions the new scheme compares favourably with the operational scheme. The area- and time averaged bias distribution in Fig 17 confirms that the new scheme represents an improvement, however the improvement is clearly most significant in the cyclonic part of the flow.

8. SUMMARY

Short range cloudiness forecasts with the operational ECMWF cloud scheme (*Slingo*, 1987) and a new scheme (*Tiedtke* 1993) have been validated in nine cases (5 winter and 4 summer cases) over Europe. The forecasted cloud fields have been compared with cloud structures in METEOSAT IR and visible imageries, surface synop observations and conceptual models. The skill of the operational scheme may be summarized in Table 1 below.

Cloud regime	**Horizontal distribution of cloudiness**	**Vertical distribution of cloudiness**
Cold front	Realistic, but overestimated cloud fraction in the upper layers	Cloud amount increases with height
Behind the cold front	Underestimated, both over land and sea	Mostly low clouds
Warm front	Underestimated	Mostly low clouds
Occlusion and hammer head region	Realistic in occlusion, but underestimated in the upper hammer head region	
Anticyclone	Underestimation of low clouds. Spurious low clouds over land due to unrealistic inversions. Overestimation of clouds associated with interactive cold fronts.	

Table 1: Summary of the performance of the cloudiness forecast with the operational ECMWF scheme for two winter cases

The available data, from all the cases, shows quite unambiguously that the new scheme has improved the synoptic representation of midle and low clouds. There are also indications of improvement in the representation of high clouds (except in the "hammer head" region in winter). This statement needs qualification, however since cirrus clouds might be difficult to detect in satellite imageries and they might be hidden from the surface observer by lower clouds.

Acknowledgements

I thank Dr G Kelly for supplying and helping me with useful software. The assistance given by Dr A Lanzinger is also gratefully acknowledged.

References

Browning, K A, 1990. Organization of clouds and precipitation in extratropical cyclones. The Erik Palmén memorial volume. American Meteorological Society, Boston.

Carlson, T N, 1991. Mid-Latitude Weather Systems. Harper Collins Academic, London.

Morcrette, J-J, L Illari, E Klinker, H LeTreut, M Miller, P Rash and M Tiedtke, 1991. Clouds and Radiation in the ECMWF model - Recent Developments. ECMWF Technical Memo no 181, Reading, UK, 48pp.

Slingo, J M, 1987. The development and verification of a cloud prediction scheme in the ECMWF model. Quart J Roy Meteor Soc, 113, 899-927.

Thorncroft, C D, B J Hoskins and M E McIntyre, 1993. Two paradigms of baroclinic-wave life-cycle behaviour. Quart J Roy Meteor Soc, 119, 17-55.

Tiedtke, M, 1993. Representation of Clouds in Large-Scale Models. Accepted for publication in Mon Wea Rev.

Økland, H, 1983. Modelling the height, temperature and relative humidity of a well-mixed planetary boundary layer over a water surface. Boundary-Layer Meteorology, 25, 121-141.

Fig 1 Infrared (IR) METEOSAT imagery of Europe 15 January 00UTC. The heavy solid lines are the 50% and 95% contour of the high cloud cover (HCC) operational 36h forecast valid at 00UTC. The thin dashed contours represent the corresponding forecast of mean sea level pressure (MSLP) in hPa.

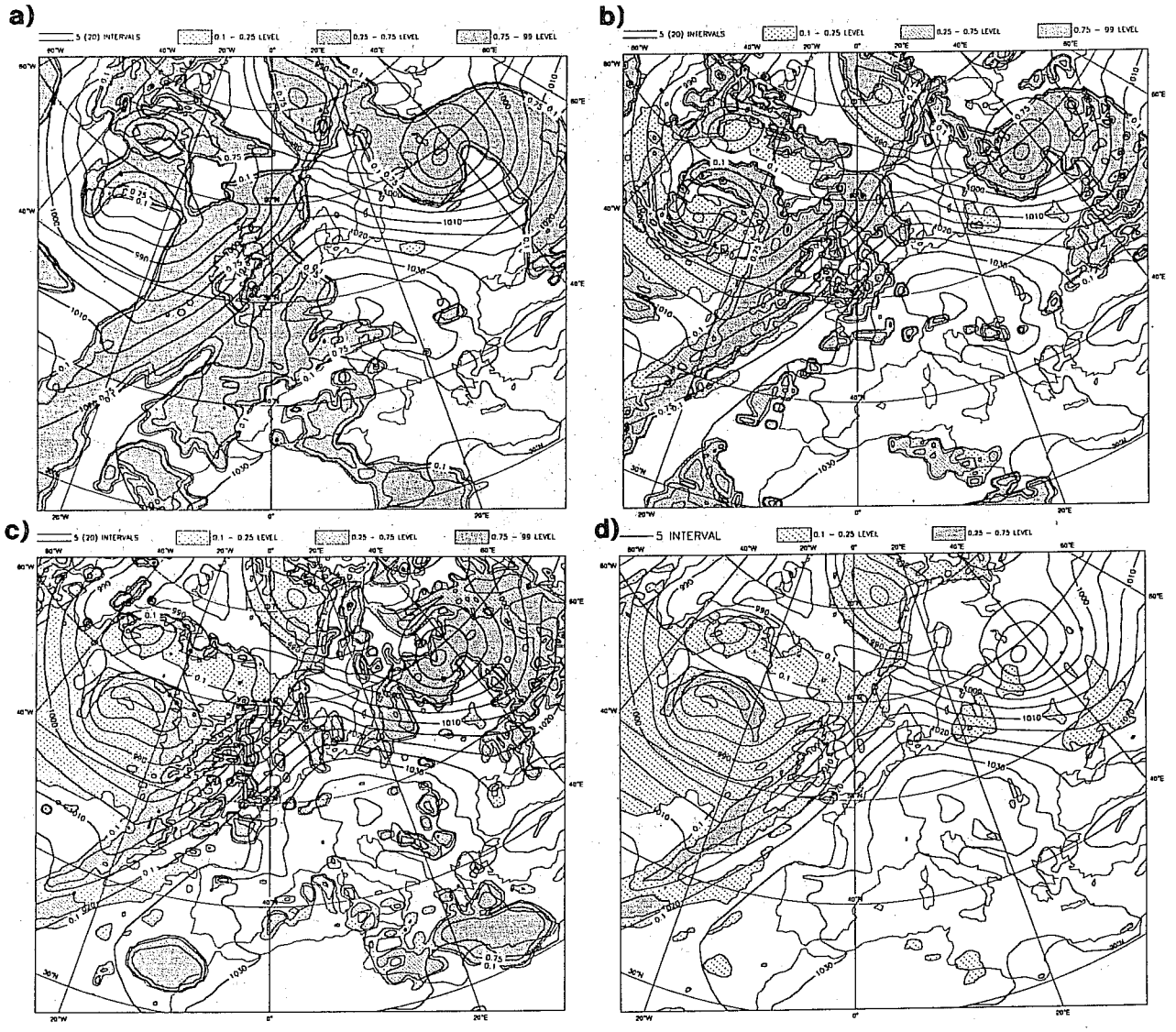

Fig 2 a) 36h prognosis of high cloud cover (HCC), with the operational scheme, valid 15 January 00UTC over Europe. Contour levels are 10%, 25% and 75%. The cloudiness field overlays the corresponding MSLP field.

b) Same as a), but with medium cloud cover (MCC).

c) Same as a), but with low cloud cover (LCC).

d) Same as a), but with convective cloud cover (CCC).

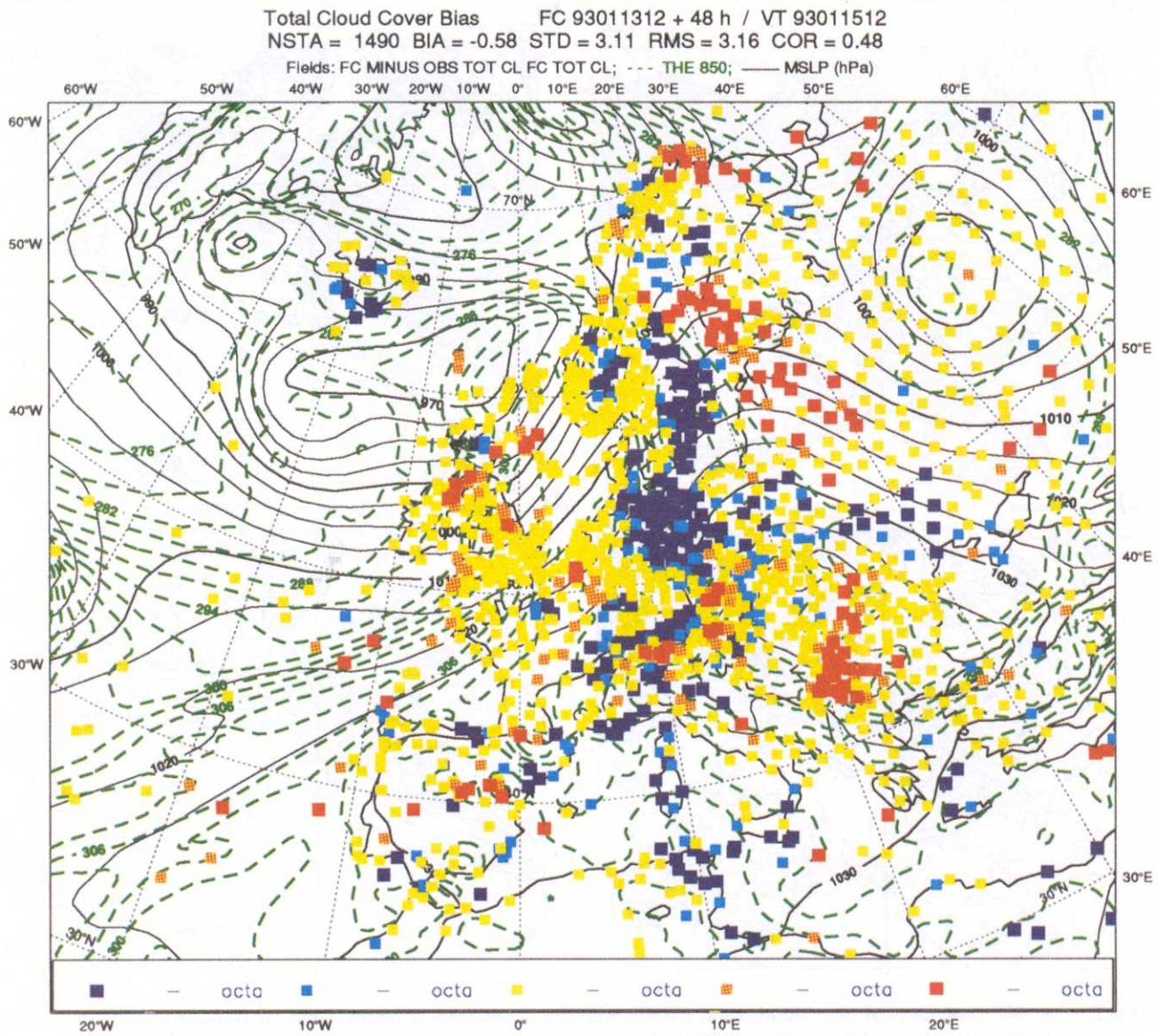

Fig 3 Difference between 48h predicted total cloud cover (TCC), valid at 15 January 12UTC over Europe, and surface observed TCC_{obs} at the same time. TCC is predicted with the operational scheme. The difference (or bias) field, Δ, is separated into 5 octa intervals, each with a different colour: $-8 \leq \Delta < -4$ navy blue, $-4 \leq \Delta < -2$ light blue , $-2 \leq \Delta \leq 2$ yellow, $2 < \Delta \leq 4$ orange and $2 < \Delta \leq 4$ red. The green dashed contours are the equivalent potential temperature field ate 850 hPa. The black solid contours are the mean sea level pressure field (in hPa).

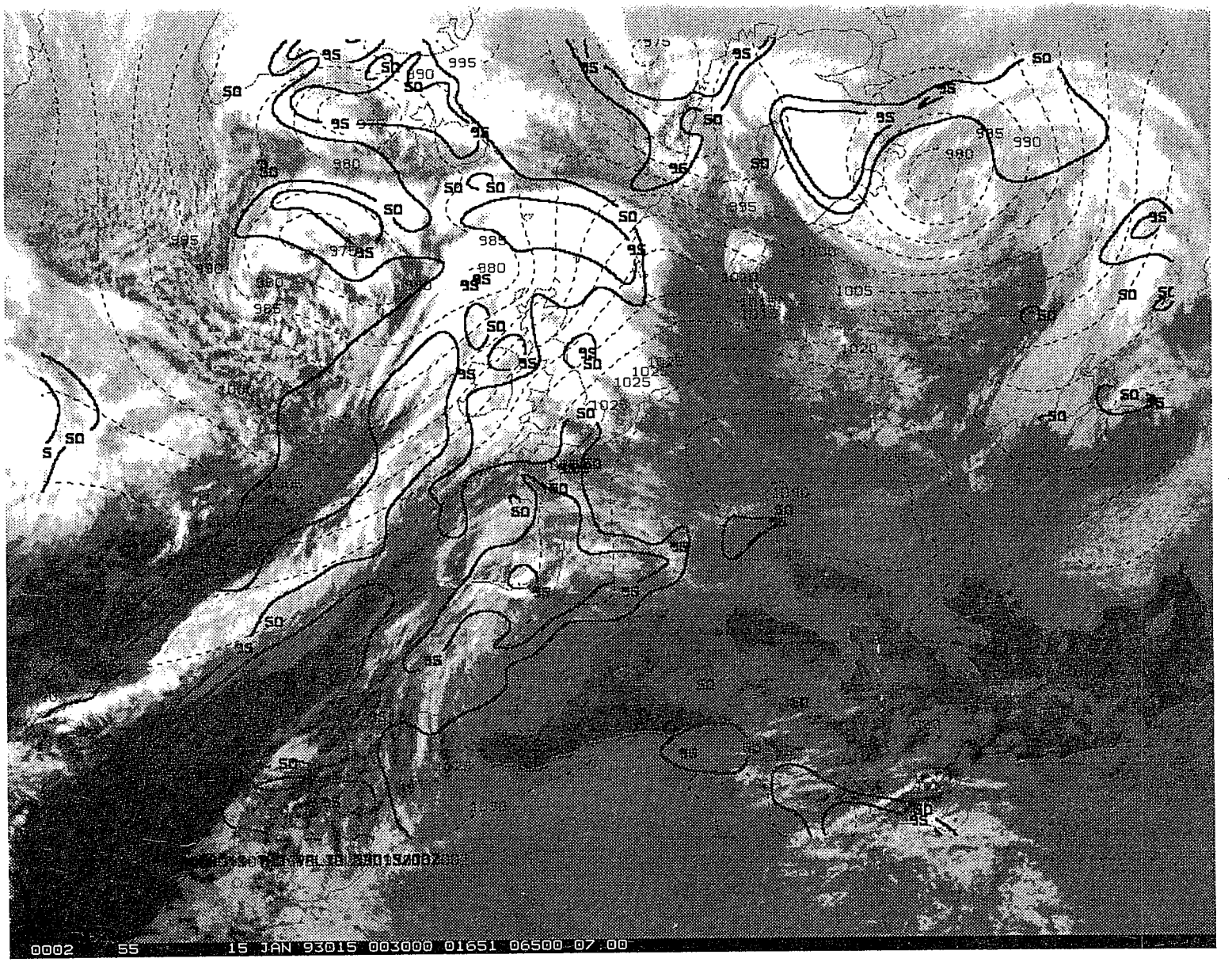

Fig 4 Same as 1, but the HCC forecast is done with the new cloud scheme.

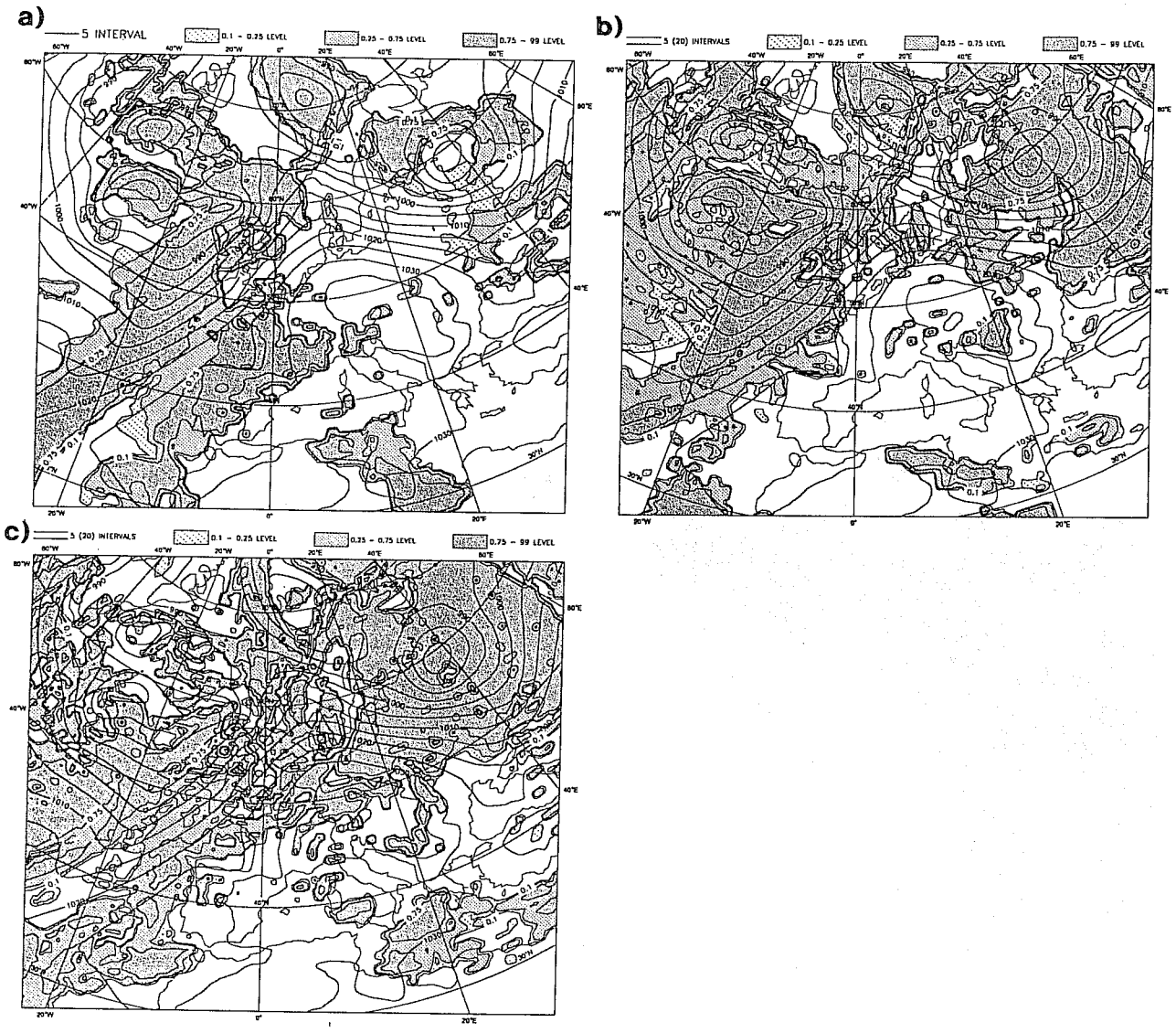

Fig 5 Same as 2 except that the cloudiness forecast is done with the new cloud scheme. Note that the new scheme does not distinguish between convective and stratiform cloudiness, which is why CCC is absent here.

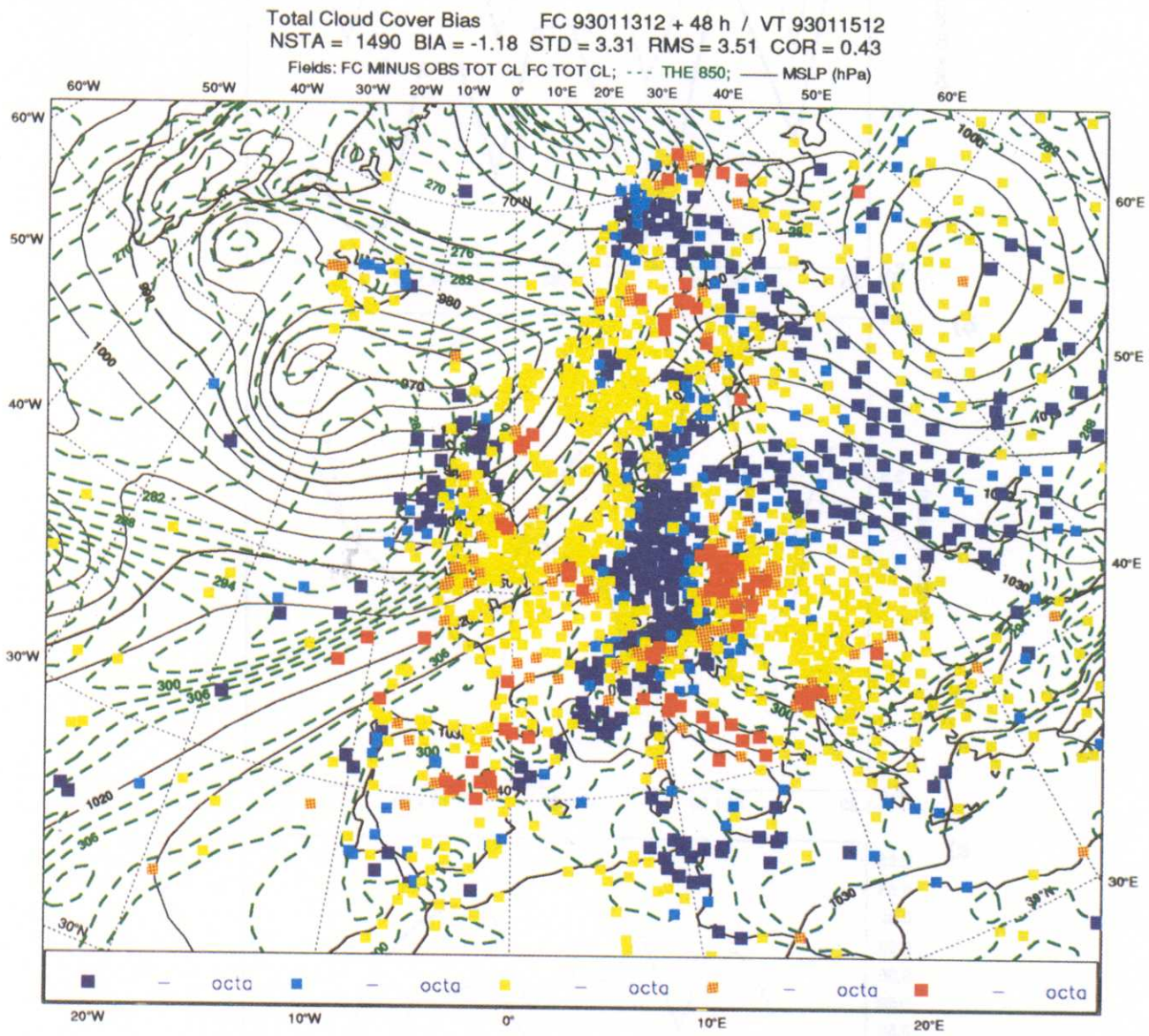

Fig 6 Same as 3 except that the cloudiness forecast is done with the new cloud scheme.

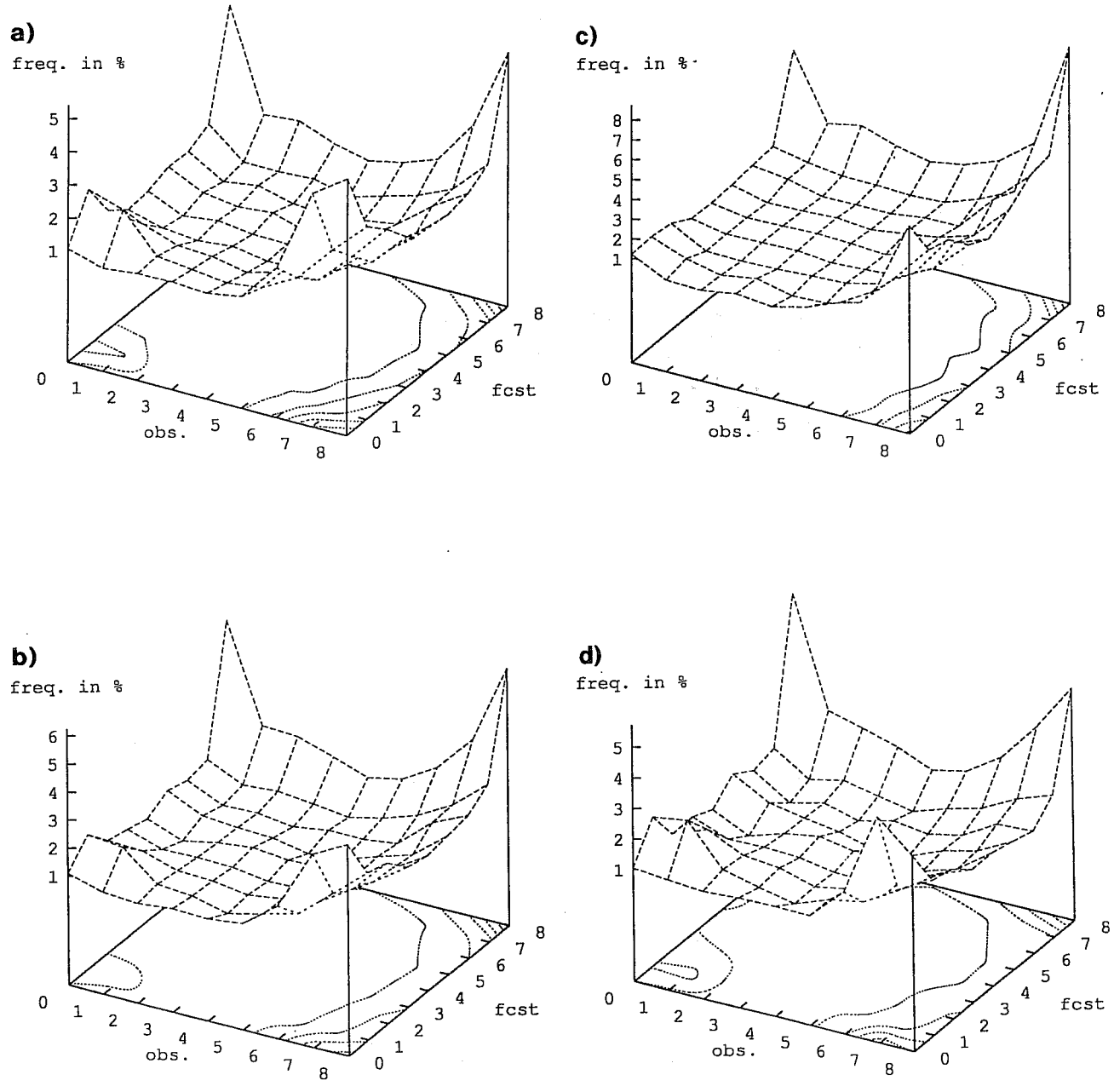

Fig 9 a) Surface and contour representation of the cross frequency matrix. The observed and forecasted cloudiness values are set along the horizontal axes and the frequency (in %) is set along the vertical axis. The forecasted frequencies are the average of the 48h forecasts in the period 15-18 January 1993. The observed frequencies are the average of the 12UTC observations in the same period.

b) Same as a), but the forecasts are done with the new scheme.

c) Same as b), but the matrix contains cyclonic points only. (A point is cyclonic if the relative vorticity at 850 hPa is greater than zero.)

d) Same as b), but the matrix contains anticyclonic points only.

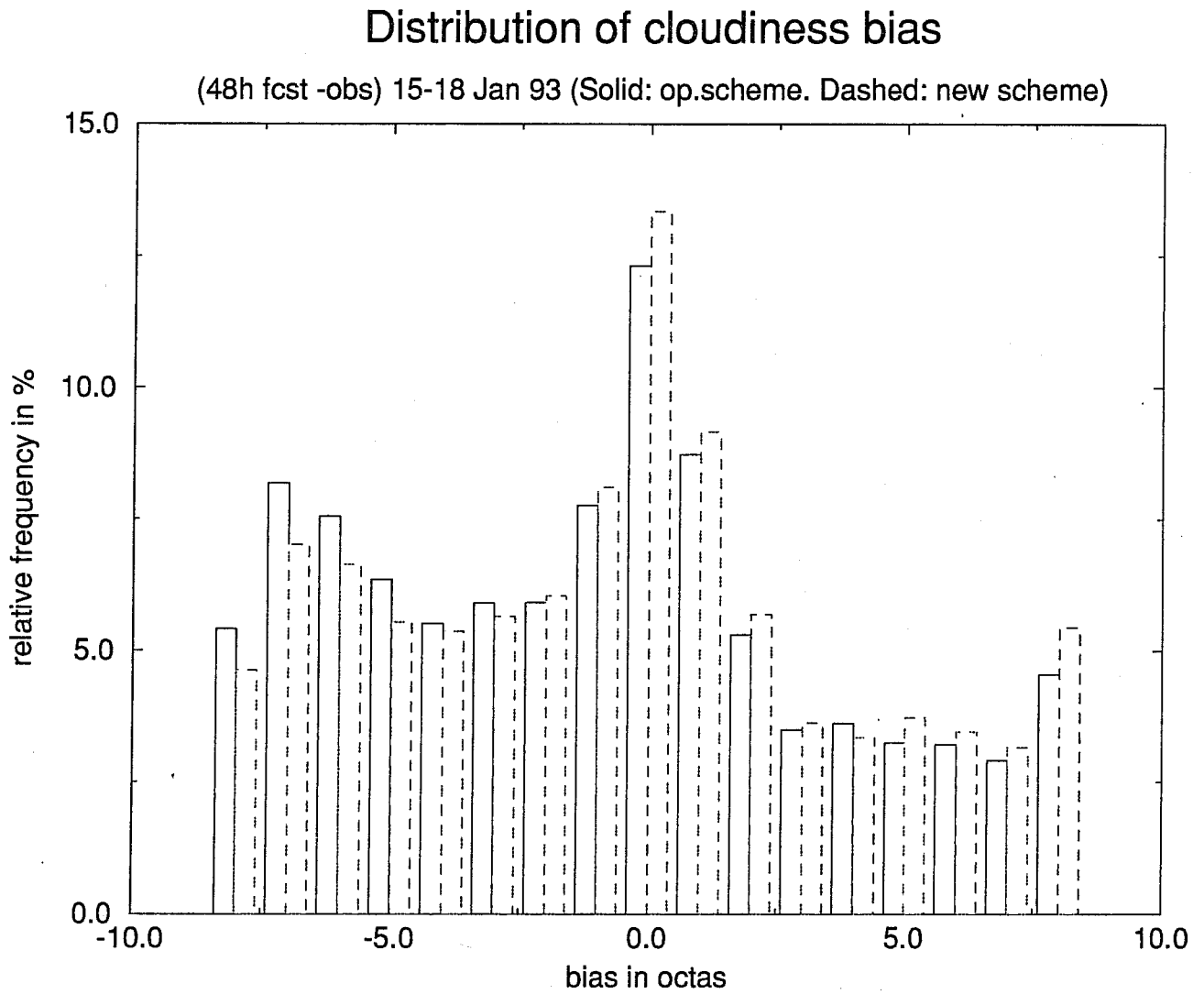

Fig 10 Solid bars: Cloud bias frequency distribution averaged over the 48h forecasts in the 15-18 January 1993 period (Bias = forecasted cloud fraction - observed cloud fraction). The solid bars are the distribution obtained from the operational forecast. The dashed bars are the distribution obtained from the "new scheme" forecasts.

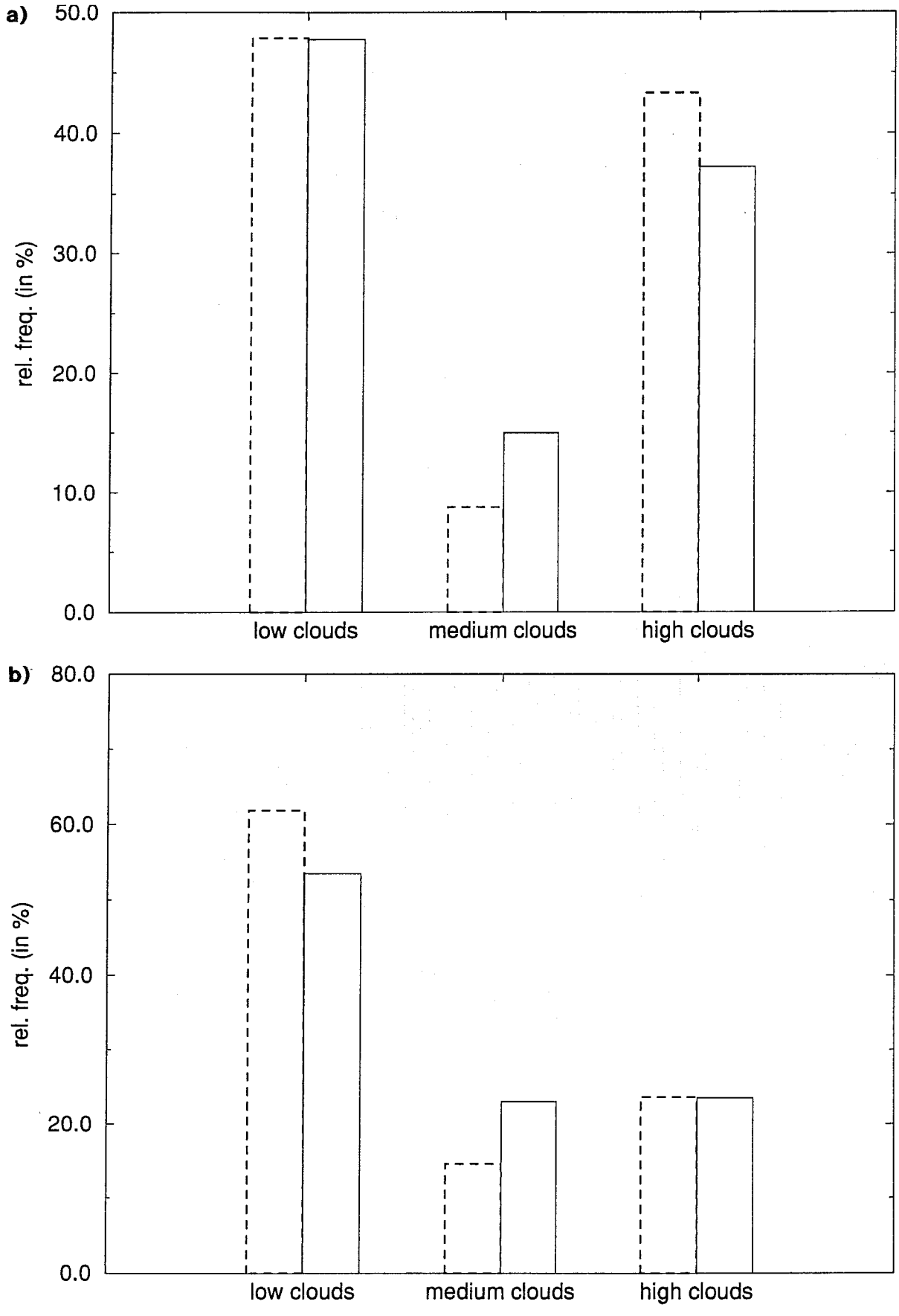

Fig 11 a) Solid bars: Forecasted cloud layer distribution for biases vith value greater than 5 octas. Dashed bars: Dominating cloud layer distribution of biases with value greater than 5 octas. (The dominant cloud layer in a column is the one with largest cloud fraction.) Both distributions are the averages over the 48h operational forecasts in the 15-18 January period. The three cloud layers are: Low clouds (1000-800 hPa), medium clouds (800-450 hPa) and high clouds (450-100 hPa).

b) Same as a), but the forecasts are done with the new scheme.

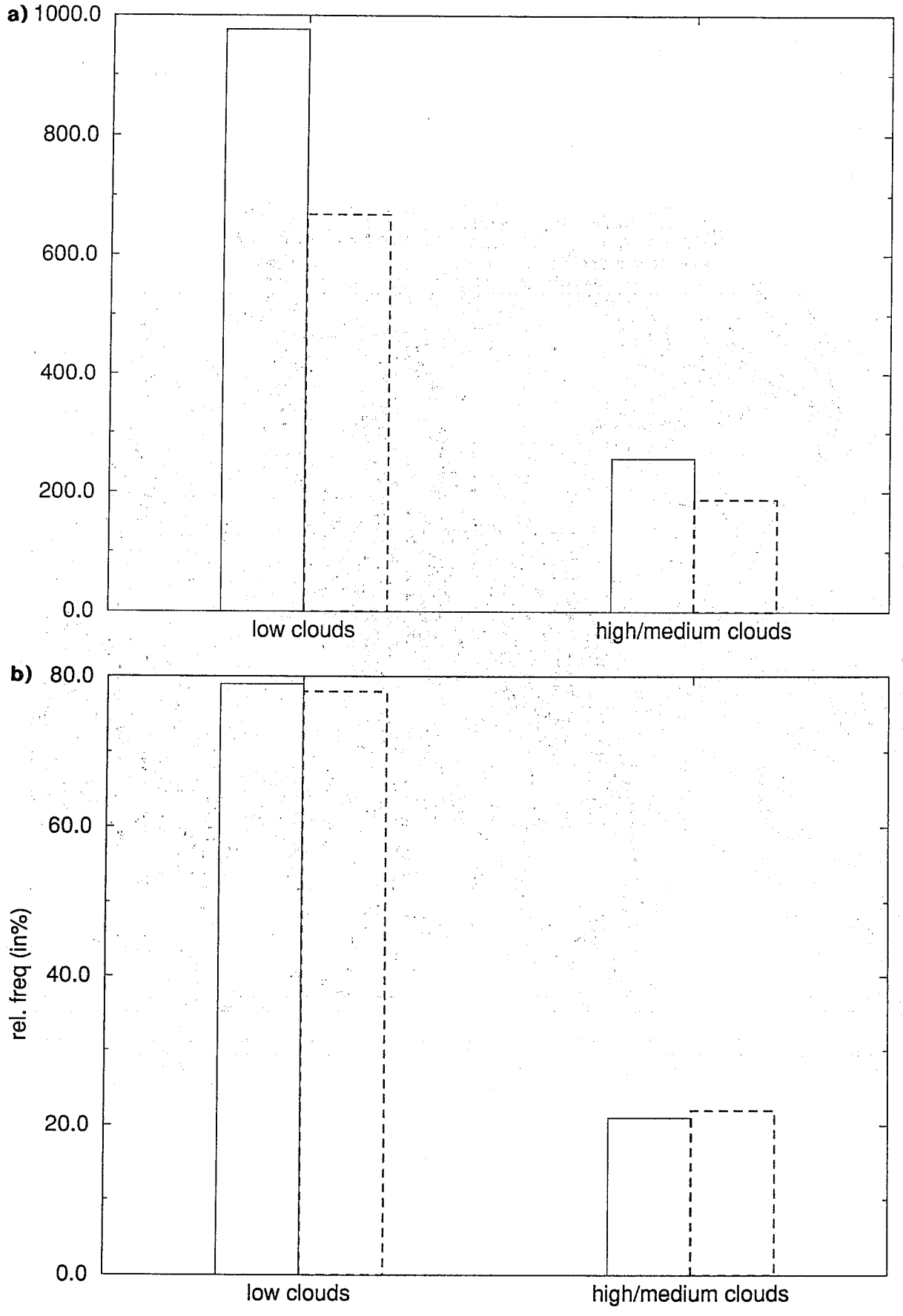

Fig 12 a) Solid bars: Observed cloud base height distribution, averaged over the 12UTC obervations in the 15-18 January 1993 period, for biases vith value less than -5 octas. The biases are calculated on basis of the operational forecast. Dashed bars: Same as solid bars, but for biases calculated on basis of forecasts with the new scheme. The observed cloud base height of the lowest significant cloud layer is divided into two classes: Low clouds (base height less than 1900 m) and high clouds (cloud base greater than 1900 m).

b) Same as a), but with absolute frequency along the vertical axis.

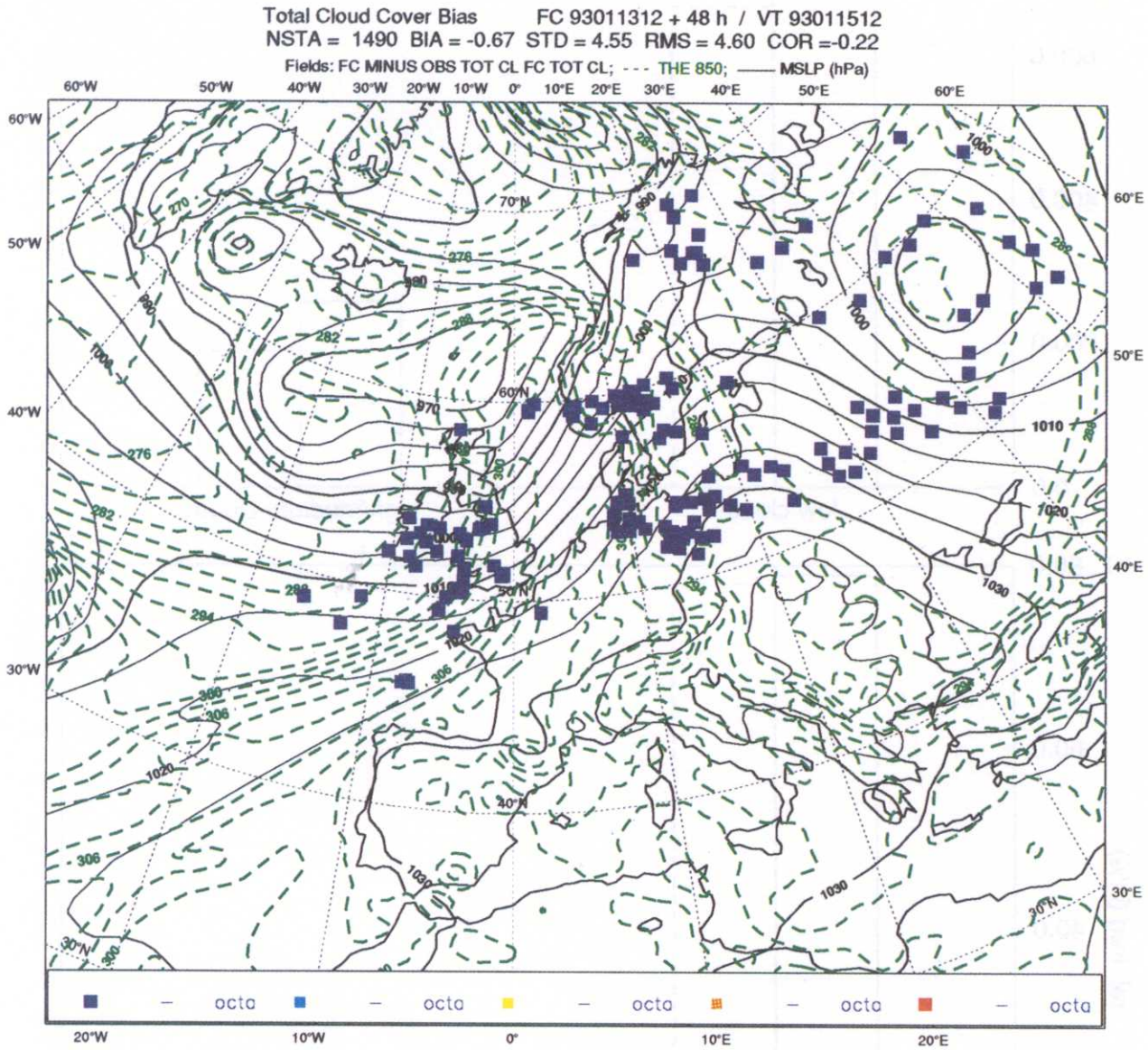

Fig 13 a) Same as 3, but only biases with value less than -5, with observed low cloud base are included.

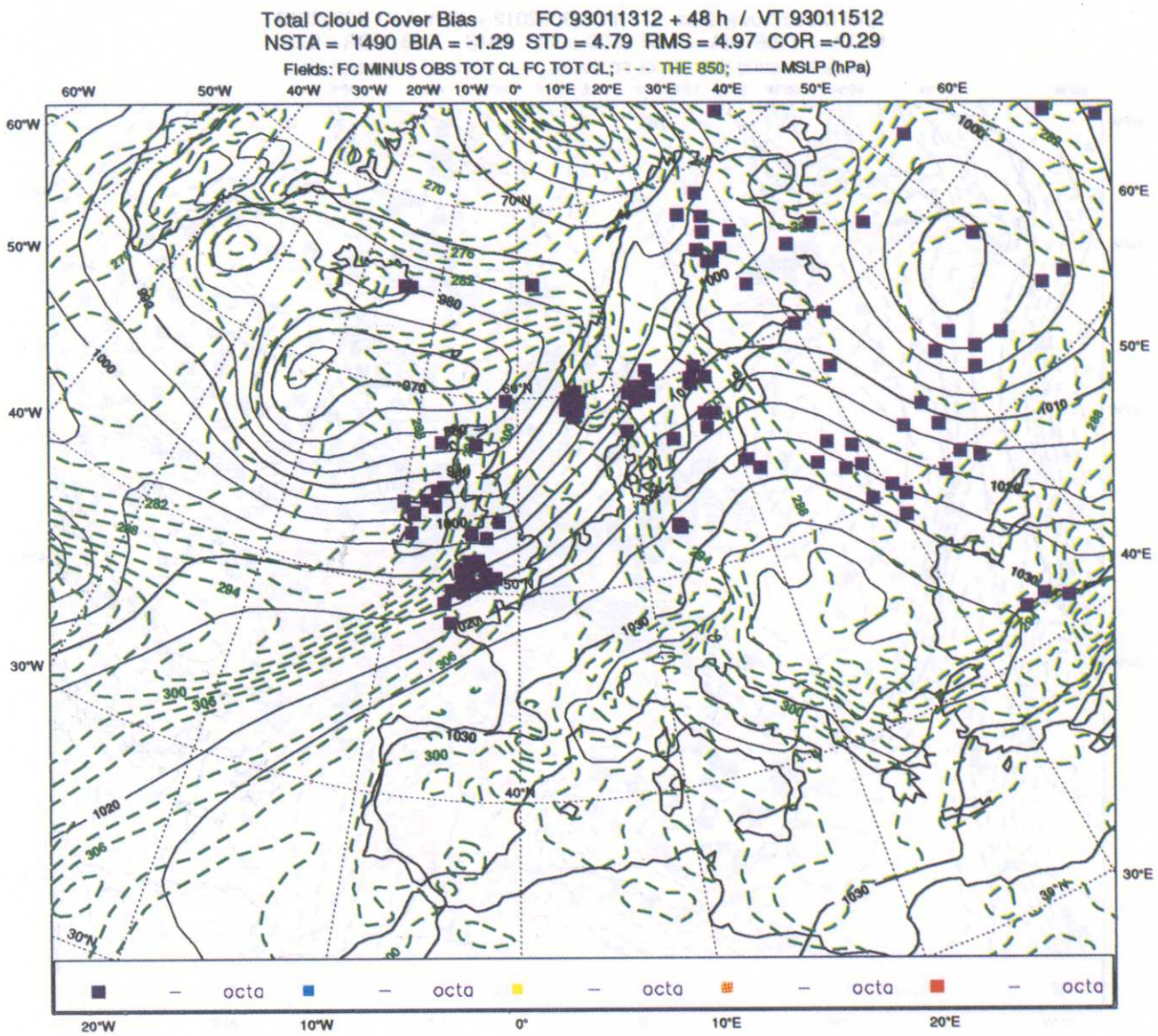

Fig 13 b) Same as a), but the forecasts are done with the new scheme.

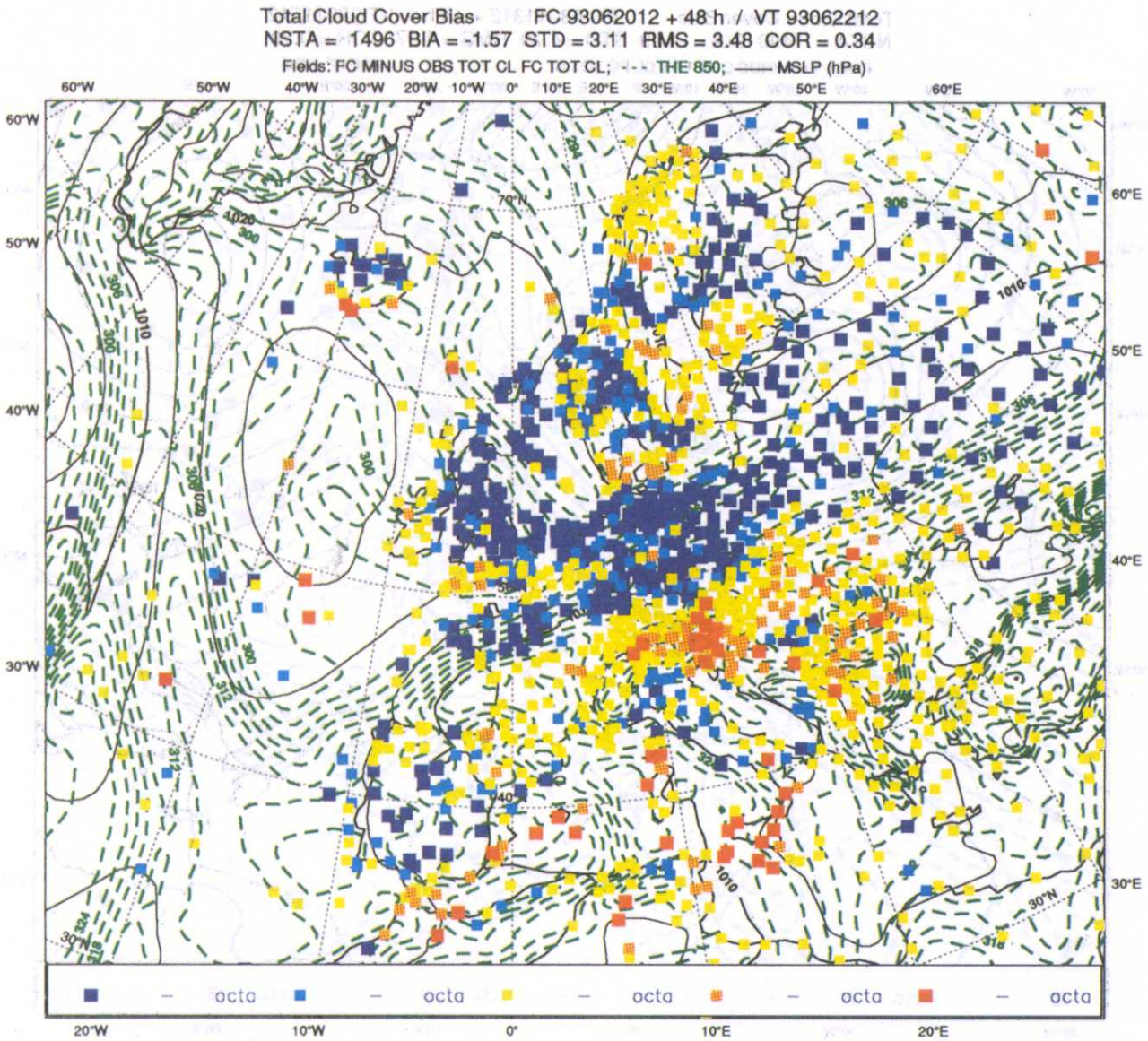

Fig 14 a) Same as 3, except except that it is a 48h forecast valid at 1200 UTC 23 June 1993.

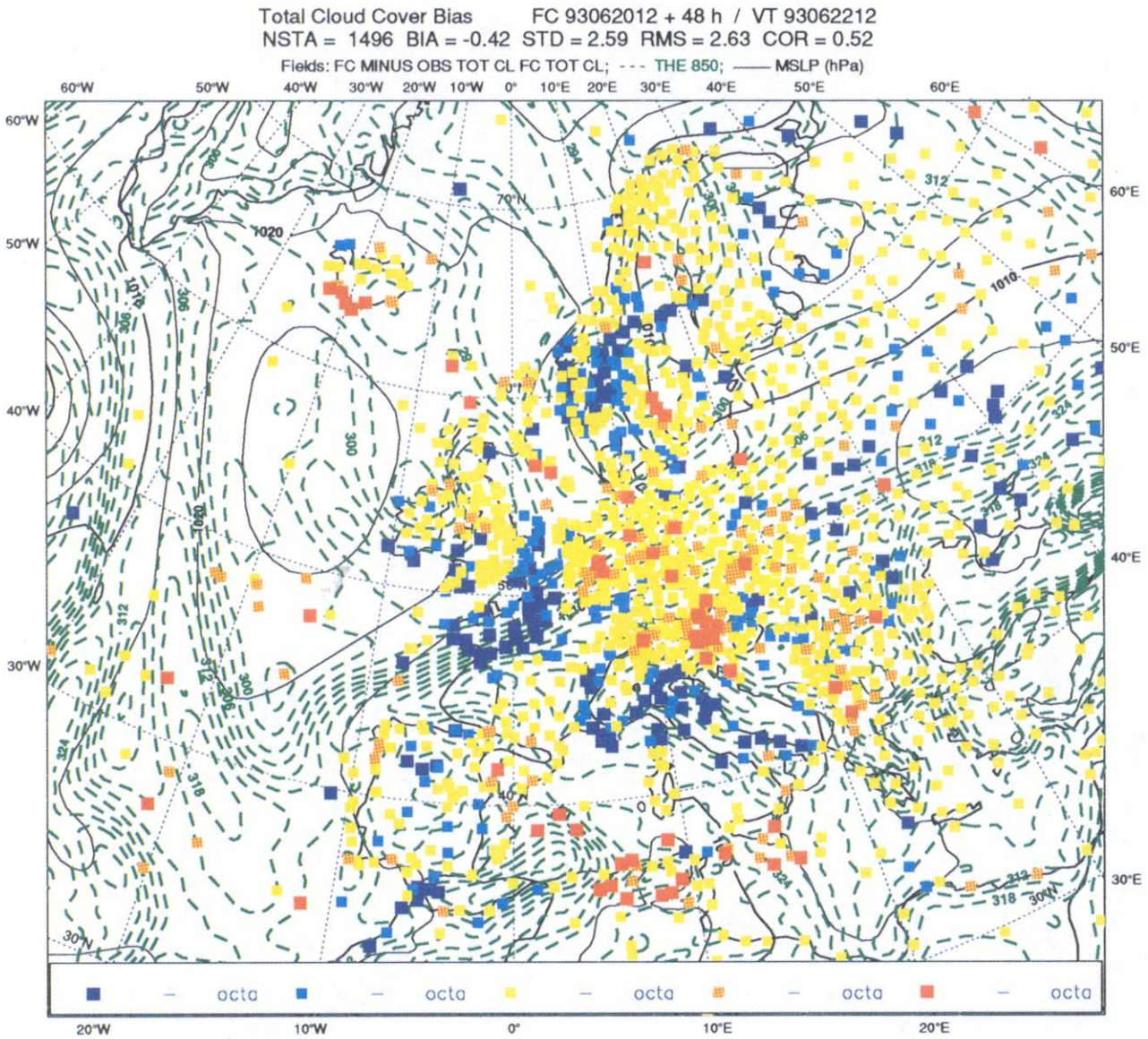

Fig 14 b) Same as a) but with the new scheme.

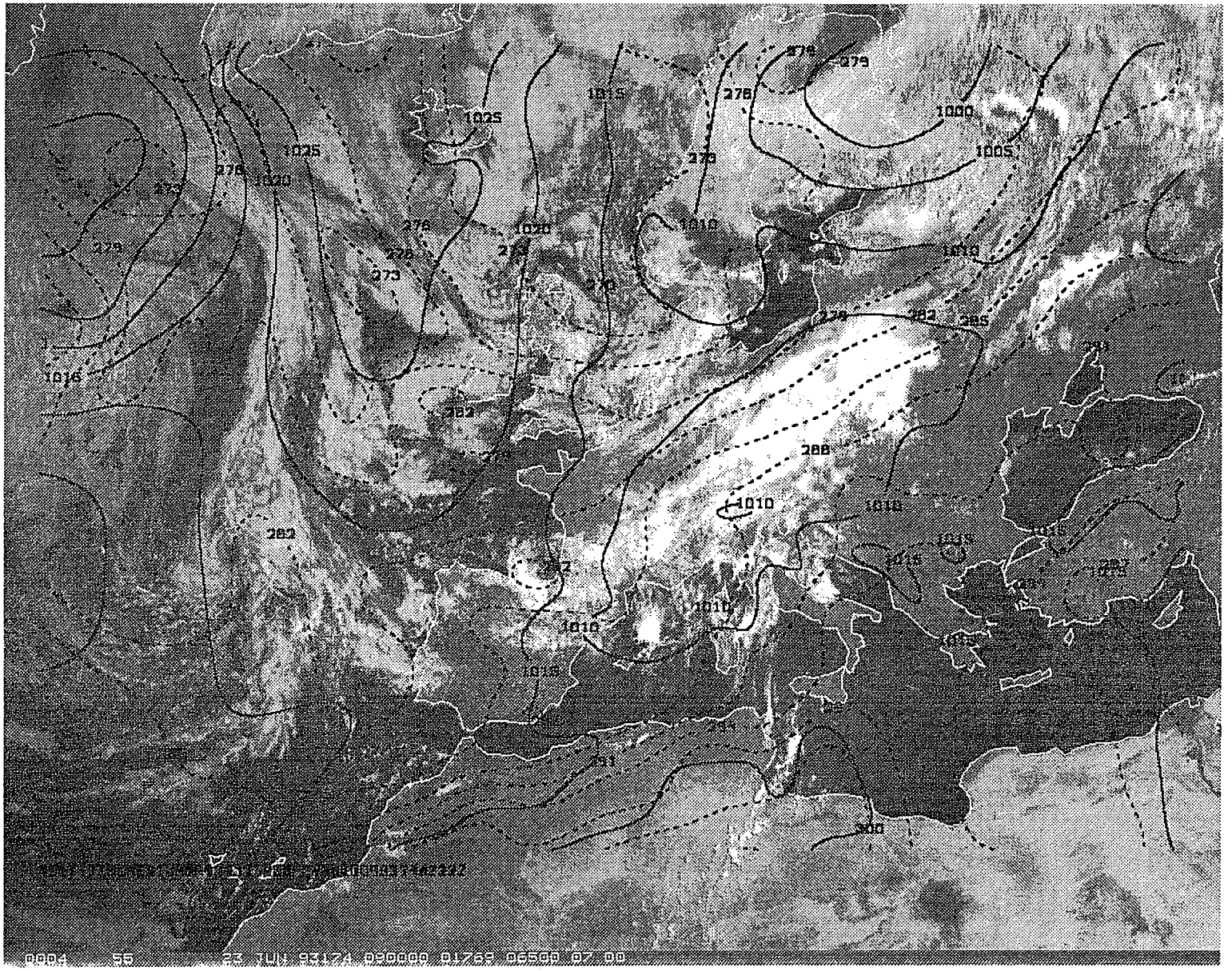

Fig 15 Visible METEOSAT imagery of Europe 23 June 900 UTC. The heavy solid and dashed contours are the operational 48h forecast of MSLP (in hPa) and temperature in the 850 hPa surface valid at 1200 UTC, respectively.

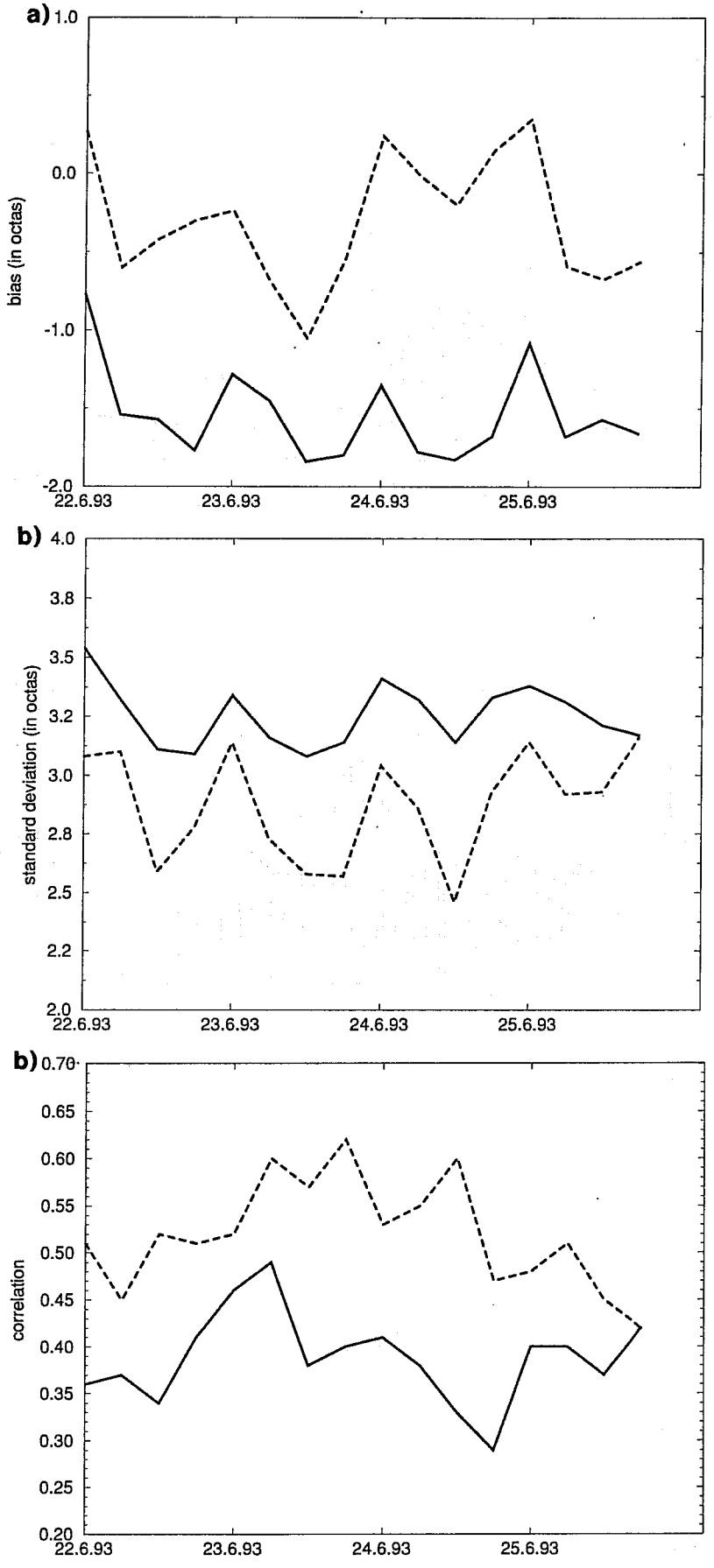

Fig 16 Same as 7, but for the four summer cases.

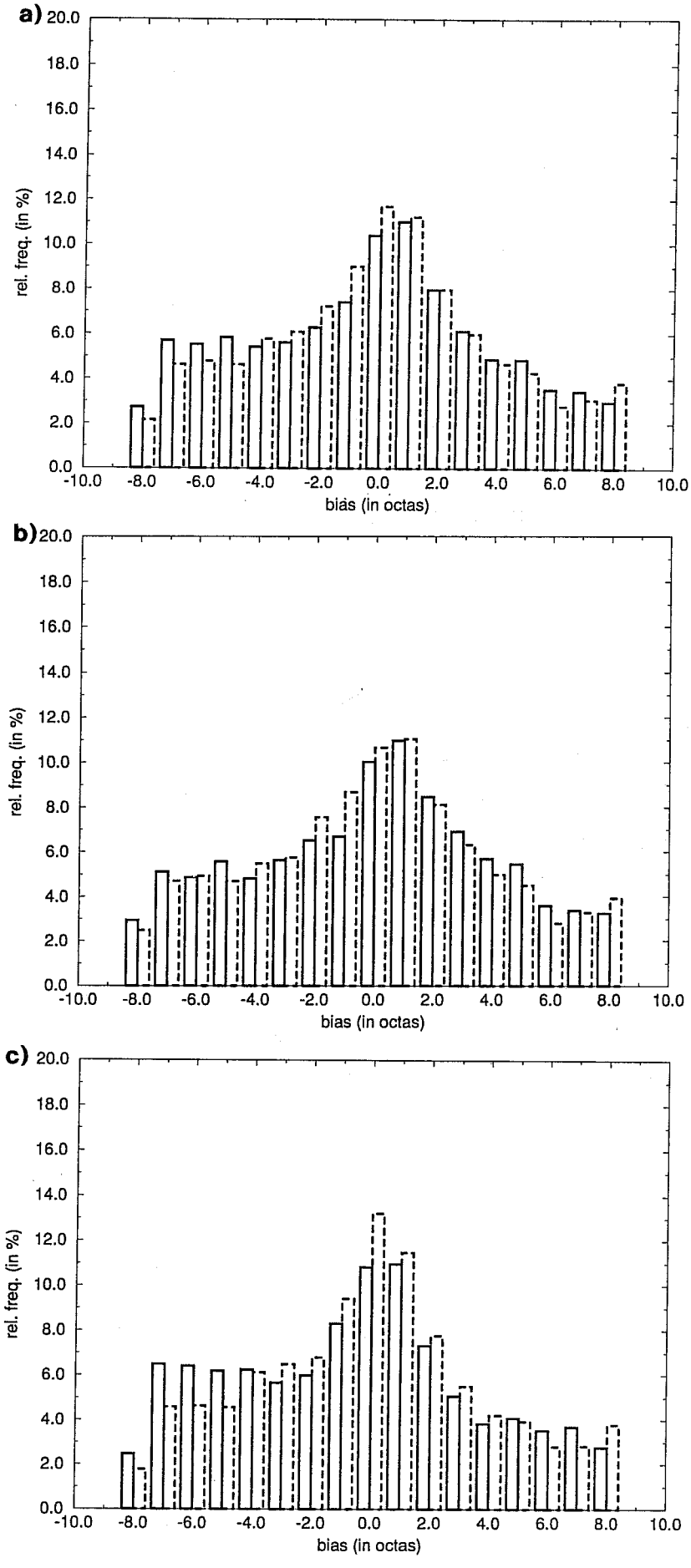

Fig 17 a) Same as 10, but for the four summer cases. b) Same as a), but anti cyclonic points only are included. c) Same as a), but cyclonic points only.